A Low-Profile Circularly Polarized Magnetic-Electric Dipole Antenna Array

Pingyuan Zhou, Mang He, Wen Tian, and Chuanfang Zhang

School of Information and Electronics
Beijing Institute of Technology, Beijing, 100081, China
py_zhou@bit.edu.cn, hemang@bit.edu.cn, 714380548@qq.com, zcf@bit.edu.cn

Abstract ─ A low-profile circularly polarized (CP) magneto-electric dipole (MED) antenna array is presented in this paper. By tilting the vertical walls of a MED with two protruded stubs being orthogonal to the horizontal patches and by using a staircase-shaped feeding strip, a wideband CP MED antenna is formed. In comparison to the conventional MED, the profile of the antenna is reduced from $0.25\lambda_c$ to only $0.07\lambda_c$ at the center frequency of the operating band. The sequentially rotated feeding (SRF) network is employed to construct a 2×2 array with enhanced 3 dB axial-ratio (AR) bandwidth. The overall size of the array is as compact as $1.33\lambda_c \times 1.33\lambda_c \times 0.07\lambda_c$, and the measured results show that the usable overlapped bandwidth of the reflection coefficient $|S11| <$ -10 dB and AR< 3 dB is 31.2%, covering 1.76 GHz to 2.41 GHz. The peak gain of the array is 12.9 dBic with the gain variation being less than 3 dB within the 1.85-2.32 GHz band, and the front-back-ratio (FBR) is greater than 20 dB. The proposed array is promising in the applications for portable and individual communication devices for wireless communications.

Index Terms ─ Circularly polarized antenna, magneto-electric dipole antenna, small size, wideband.

I. INTRODUCTION

As a type of wideband complementary antenna, the magneto-electric dipole (MED), which was first proposed by Luk in 2006, has attracted widespread interests in recent years [1-15]. The MED antenna has many advantages such as wide bandwidth, symmetrical beam, low cross-polarization level, and stable gain, etc. However, the traditional MED antenna usually has a relatively high profile of about 0.25 wavelengths at the center frequency of the operating band, which may limit its application in many portable communication systems.

A lot of works have been conducted to lower the profile of the MED antenna. In [2], the height of a wideband MED is reduced to $0.2\lambda_c$ by attaching two extra inverted-L-shaped wires above the shorted bowtie patches. In [3,4], a horizontal planar dipole and a pair of vertical folded patches are used to further reduce the antenna profile to $0.17\lambda_c$, and 55% 10 dB impedance bandwidth is reached. In [5], the profile of the MED is lowered to $0.156\lambda_c$ by bending the vertical shorted patch to a triangular shape, and a very wide bandwidth of 86.2% is obtained. A new MED with the height of $0.16\lambda_c$ is presented in [6], although the structure of the antenna is much simple than those in [2-5], the antenna still has wide impedance band- width of 45%. In [7], by replacing the traditional quarter-wave vertical shorted patch with a bent one of an obtuse-triangle- shaped cross section, the antenna's profile is lowered down to $0.097\lambda_c$, at the expense of reduced -10 dB $|S11|$ bandwidth of 28.2%. The thickness of the MED is reduced to only $0.035\lambda_c$ in [8], but the bandwidth decreases to 20.7% and the FBR rises to 16 dB. [9-11] give the dielectric substrate loaded or substrate integrated MED, and the profiles of the antennas can be reduced to the order of 0.08 to $0.11\lambda_c$. However, these antennas suffer from complexity in construction of the ground reflector and in assembling process, relatively high fabrication cost and sensitivity to environments, narrow bandwidth, and reduced gain in comparison with the air-support metal MED antennas.

In contrast to the linearly polarized antennas, wideband CP antennas are often required in many communication systems to avoid multipath effects and mitigate the polarization mismatch. Recently, [12-15] have presented several wideband CP MED antennas. In [12], a CP MED antenna is designed by combing two bowtie patch antennas with two electric dipoles. It is fed by a Wilkinson power divider, and 33% overlapped -10 dB $|S11|$ and 3 dB AR bandwidth is achieved, but the height of the antenna is $0.25\lambda_c$. In [13], a $0.21\lambda_c$-thick wideband crossed- dipole loaded CP MED is proposed, and the usable bandwidth is 26.8%. In [14], two symmetric electric dipoles, two vertical patches, and a cavity with two gaps are combined to provide 65.1% overlapped CP bandwidth, but the antenna's profile is as high as $0.27\lambda_c$. In [15], two L-probe fed CP MED antennas, operating respectively at the microwave and millimeter-wave bands, possess the overlapped bandwidths of 47.7% with the $0.29\lambda_c$ profile and 41% with the $0.15\lambda_c$-profile. Although wide CP bandwidths have been obtained in [12-15], the heights of the MED antennas are still quite high; this is undesirable for some

Submitted On: May 6, 2019
Accepted On: September 10, 2019

portable devices.

In this paper, a low-profile wideband CP MED antenna array is proposed for portable or individual wireless devices, in which compactness and light-weight is one of the most important requirements. Based on the proposed single-fed CP MED antenna with wide impedance bandwidth, which has a much lower profile of $0.07\lambda_c$ as compared with the traditional $0.25\lambda_c$-thick MED antenna, a 2×2 array is constructed by using the sequentially rotated feeding (SRF) technique. The use of SRF network [16,17] further enhances the polarization purity and AR bandwidth, and the overlapped AR< 3 dB and |S11|< -10 dB bandwidth can be greater than 30%. Within the operating band, the gain variation is less than 3 dB from 1.85 to 2.32 GHz, showing a 22.5% 3 dB gain bandwidth.

II. ANTENNA ELEMENT

A. Antenna configuration

The geometry of the proposed MED antenna element is shown in Fig. 1. Two metallic patches with each dimension of $L_1 \times W_1$ and being parallel to the ground, together with two attached stubs with the each size of $L_2 \times W_2$ protruding along the *y*-direction, form an electric dipole (ED). The position of the stub measured from the inner edge of the patch is W_3, and the gap width between the two arms of the ED is S. In Fig. 1 (c), two inclined metallic patches connect the inner edges of the two horizontal patches to the ground, in which α denotes the included angle between the slanted patches and ground, and H is the height of the antenna. Similar to the conventional MED antenna [1], [7], the shorted inclined-patches, the ground, and the aperture between the ED's two arms, form an equivalent magnetic dipole (MD). The feeding line of the antenna is a staircase-shaped metallic strip, as shown in Fig. 1 (d), which consists of four parts. The first part is a vertical strip with the length of l_1, and it connects to the intersection line of the horizontal patch and the inclined shorted patch. The second part is a horizontal strip with the length of l_2, and the third part, with the length being l_3, is parallel to another inclined shorted patch. The first three parts share the same width of W_{f1}. The fourth part of the feeding line is a vertical strip with the shape of an inverted trapezoid. The lengths of the top and bottom bases, and the height of the trapezoid are W_{f1}, W_{f2}, and l_4, respectively. The antenna element can be fed by connecting the inner conductor of a SMA connector to the bottom base of the trapezoid and attaching the outer conductor to the ground. The third part (l_3) works as a microstrip line and the distance between the line and inclined-patch can be determined by the basic formula for microstrip line design. It is noted that in this section the size of the ground is set to G= 150 mm ($0.95\lambda_c$) for analysis the properties of the single MED antenna element.

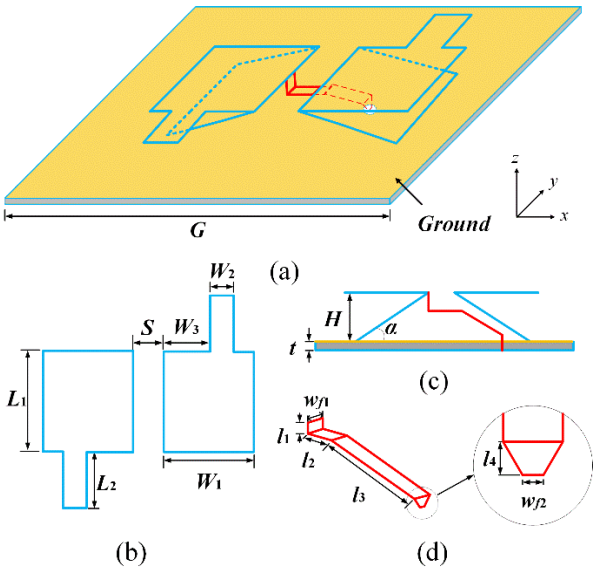

Fig. 1. Configuration of the proposed MED antenna element. (a) Perspective view, (b) top view, (c) side view, and (d) the feeding strip. Optimal dimensions of the antenna element (unit: mm): L_1=51, L_2=13, W_1=51, W_2=10, W_3=25, S=6, H=10, G=150, l_1=2, l_2=6, l_3=17.3, l_4=2, t=1, w_{f1}=2.1, w_{f2}=1.3. α=20.3°.

B. Operating principles

As shown in Fig. 1, it is apparent that both the equivalent electric currents of ED and the equivalent magnetic currents of the MD are *y*-directed. In the *xz*-plane, both the electric field radiated from the ED and that from the MD have the same shape of figure "O", although they are spatially orthogonal. In addition, there is an inherent 90° phase difference between these two sets of electric fields since one of them is radiated from an ED and the other one is produced by an equivalent MD [18]. Thus, good CP radiation can be generated in the entire *xz*-plane. However, if we consider the presence of the ground plane, in the *xz*-plane the electric field from the ED will be shorted at the ground plane because it is tangential to the ground; while the electric field from the MD will not since it is normal to the ground. Therefore, given the existence of ground plane, the total electric field in the upper half *xz*-plane is the superposition of the field from the ED with the shape of half figure "8" and that from the MD with the shape of half figure "O". This indicates that low AR can be kept in the upper half *xz*-plane except the region near the ground plane.

In the *yz*-plane, the electric fields from the ED and MD are still orthogonal in space and quadrature in phase but both radiation patterns are like figure "8". The electric field from the ED will be enhanced near the ground, because it is vertically polarized with respect to the ground plane in the *yz*-plane; while the electric field from the MD will be shorted since it has only tangential

component to the ground. So, the total radiated electric field in the upper half *yz*-plane is still the sum of the field from the MD with the shape of half figure "8" and the field from the ED with the approximate shape of half figure "O". It is seen that the proposed MED antenna can produce good CP and symmetrical radiation in the upper half space over a wide frequency range, if the ED and MD are excited with nearly the same magnitude.

To better understand the operating principle, the current distributions on the ED patches and the electric field vectors in the gap at different time instants within one period T are shown in Fig. 2. At the instant t=0, the current on the ED patches is dominated along +y-axis, while the electric field in the gap is minimized, which indicates that the ED is strongly exited. At t=T/4, the electric field in the gap is strong along -x-axis, while the current on the ED patches is weak, which means the MD is strongly excited at this instant. As seen in Figs. 2 (c) and (d), in the next half period, the current and electric field distributions repeat the ones at t=0 and t=T/4 but with opposite directions. It is clear that the circulation of the electric current and field in one period meets the requirement for possible CP radiation.

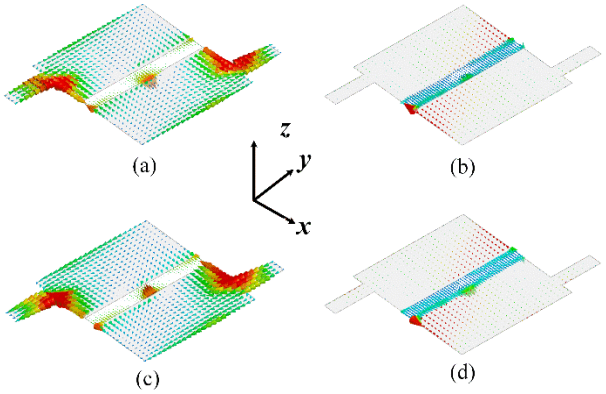

Fig. 2. Current and electric field distributions of the proposed antenna at different time instants: (a) t=0, (b) t=T/4, (c) t=T/2, and (d) t=3T/4.

C. Antenna element performance and parametric studies

From Fig. 1, two resonant frequencies can be predicted existing in the structure of the antenna. The ED determines the lower resonant frequency f_L since it has a long current path, and the higher one f_H is dependent of the effective length and width of the equivalent MD. The electric current length of the ED is mainly affected by L_1+L_2, the effective length and width of the MD is determined by the parameters L_1, S, and W_1, while S also significantly affects the coupling between the ED and MD. Therefore, parametric studies are carried out on the three key sizes of L_2, W_1 and S in order to optimize the performance of the antenna, and only one parameter varies while the others are kept unchanged in each of the following analyses, and the final optimum geometrical sizes for the MED antenna are listed in the caption of Fig. 1.

The variations of |S11|, AR and gain of the antenna versus L_2 are shown in Fig. 3 (a). It is seen that both AR and |S11| are sensitive to the variation of L_2. When L_2 increases, f_L is shifted downward since the current path of the ED is elongated, whereas f_H almost remains unchanged. The minimal AR frequency is lowered as well, which results in misalignment of the AR and |S11| bandwidths. Besides, the peak gain decreases by 0.6 dB or so as L_2 is increased from 10 mm to 16 mm. Thus, in order to obtain a wide overlapped AR and |S11| bandwidth and high gain, the stub length L_2 is set to 13 mm.

Figure 3 (b) shows the effects of the arm length of the ED on the performance of the antenna. It is observed that the two resonant frequencies are shifted downward with the increased W_1, which indicates that the current path along the ED and the effective length of the MD are both elongated by increasing W_1. The antenna appears to be mismatched at low frequency, and the AR and |S11| operating bands become misaligned. Moreover, f_H shifts downward more strongly than f_L does, which means that W_1 has more significant effects on the MD

The effects of gap width S between two ED patches on the antenna's performance is illustrated in Fig. 3 (c). It is clearly that the large S will cause the higher resonant frequency move upward significantly, while the low resonant frequency remains almost unchanged. But when S increases, the coupling between the two arms of the ED becomes weak, and impedance mismatch is seen near the frequency of f_L. The AR and gain of the antenna are almost not affected by changing S, which indicates that the excitation magnitude and phase relationship between the ED and MD is almost independent of S.

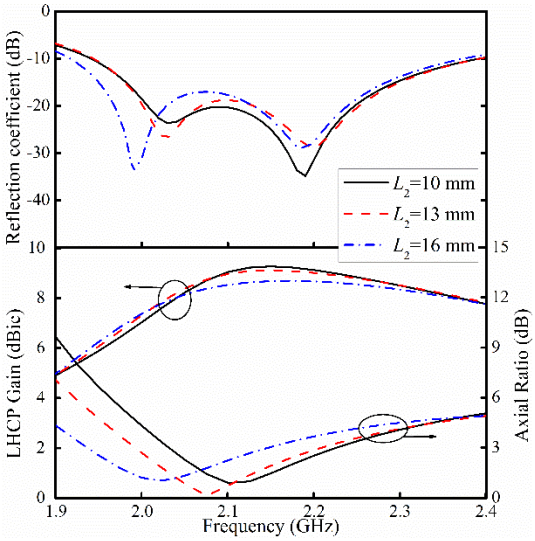

(a)

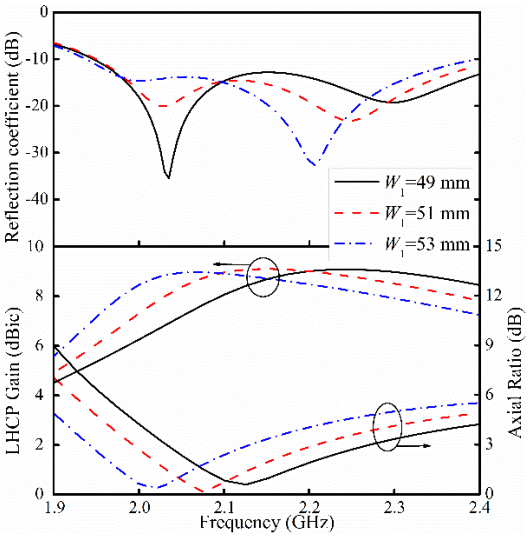

(b)

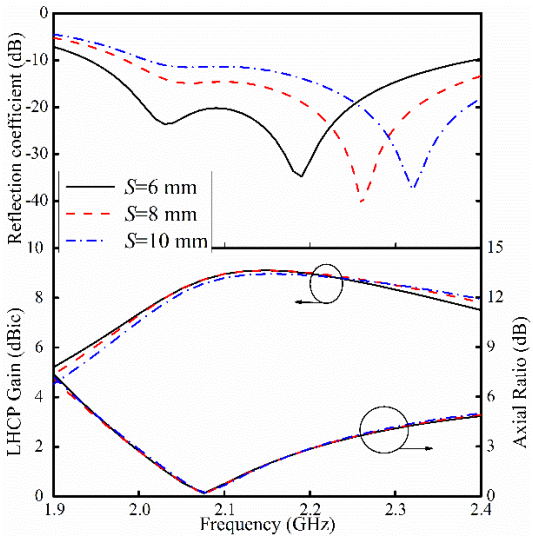

(c)

Fig. 3. Effects of different geometrical parameters on the performance of the MED antenna element: (a) L_2, (b) W_1, and (c) S.

With the optimum geometrical sizes, the MED antenna has 20.3% overlapped |S11|< -10 dB bandwidth from 1.95 GHz to 2.39 GHz and 10.5% AR< 3 dB bandwidth from 1.99 GHz to 2.21 GHz, respectively. The peak gain of the antenna is 9.11 dBic, and the variation of the gain is less than 3 dB from 1.97 GHz to beyond 2.5 GHz.

III. ANTENNA ARRAY DESIGN AND PERFORMANCE

A 2×2 array is constructed by four proposed MED antenna elements, denoted by A1 to A4, and the layout of the array is shown in Fig. 4. The four antenna elements are placed above the top surface (as the ground plane of the antenna) of a double-sided copper clad laminate, and the SRF network is etched on the bottom surface to excite the array. The relative permittivity, loss tangent, and thickness of the dielectric substrate are ε_r=3.5, tanδ=0.002, and t=1 mm, respectively. The SRF network is composed of two-stage Wilkinson power dividers to provide wideband and stable power division ratio and phase difference between the antenna elements. Each antenna element is excited by connecting the output of the power divider to the inverted trapezoid, i.e., the fourth part at the end of the feeding strip, through a metal probe. For a left-handed circular polarization (LHCP) design, the elements $A1$ to $A4$ rotate clockwise, and the feeding phase for each element is 90° lag to that of the former one. The spacing between two neighbor elements is D= 84 mm (0.58λ_c), so the overall size of the array is about 190 mm×190 mm×11 mm (1.33λ_c×1.33λ_c×0.07λ_c).

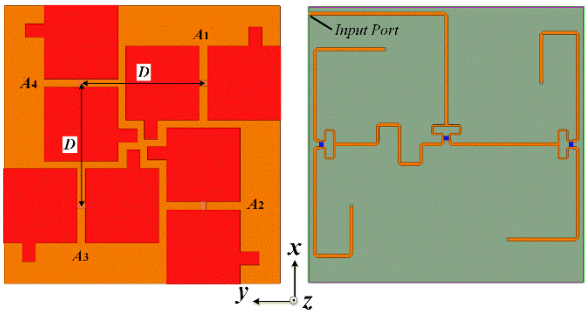

(a) (b)

Fig. 4. Layout of the 2×2 array: (a) top view and (b) SRF network composed of two-stage Wilkinson power dividers.

Parametric studies of L_2, W_1 and S are carried out to study their effects on the performance of the array. The variations of the AR and |S11| of the array versus L_2 are shown in Fig. 5 (a). The relationship between L_2 and the two resonant frequencies is complicated in array environment. When L_2 increases, owing to the stronger mutual coupling between antenna elements, f_L shifts upwards first and then moves to lower frequency slightly while f_H is increased continuously, so the two resonant frequencies depart from each other. Meanwhile, the AR is seen slightly increased at high frequency, and the gain of the array decreases quickly if L_2 is enlarged to 16 mm.

As shown in Fig. 5 (b), when W_1 is increased from 49 mm to the optimum value of 51 mm, f_H shifts down from 2.25 GHz to 2.2 GHz, and the impedance matching is improved. The lower resonant frequency f_L shifts upward slightly; and as W_1 increases to 53 mm, f_H moves to a higher frequency with f_L being almost unchanged. Meanwhile, a large loss of gain of the array at higher frequency is observed. Based on these findings, it is evident that overlarge value of W_1 cannot be chosen to construct the compact array, since large W_1 leads to small

edge-to-edge spacing between the antenna elements and then causes strong mutual coupling.

Figure 5 (c) gives the effects of *S* on the array's performance. It can be seen that continuously increased *S* does not lower down the two resonant frequencies monotonically as the single antenna does because mutual coupling among the antenna elements is strong due to the large *S*. At the same time, it is also observed that the gain is reduced at the high frequency band with the increased *S*.

With the optimum geometrical sizes of the antenna element, the 2×2 array has a more than 35% |*S*11|<-10 dB bandwidth from 1.76 GHz to 2.50 GHz, an AR< 3 dB bandwidth of 33% from 1.74 GHz to 2.42 GHz, and 3 dB gain bandwidth of 22.5% from 1.88 GHz to 2.37 GHz.

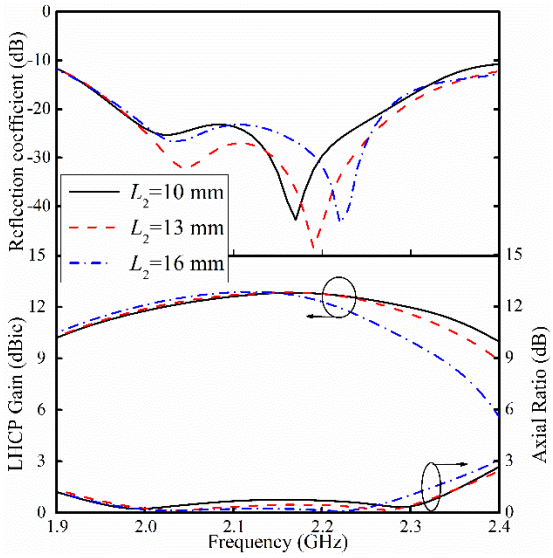

(a)

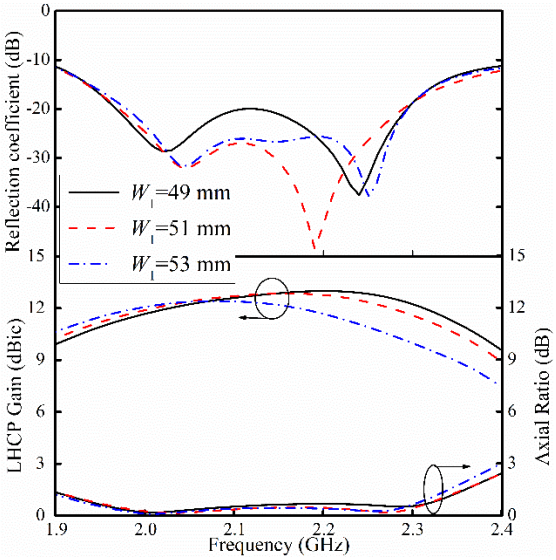

(b)

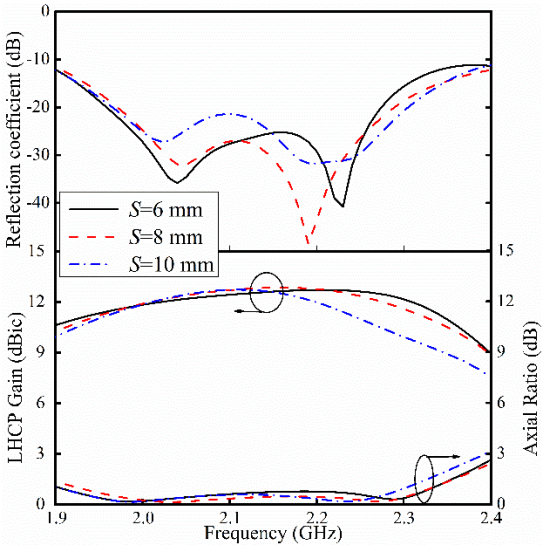

(c)

Fig. 5. Effects of different geometrical parameters on the performance of the MED antenna array: (a) L_2, (b) W_1, and (c) *S*.

V. EXPERIMENTAL VERIFICATION

A 2×2 CP MED array is fabricated, as shown in Fig. 6. The array element has the optimum dimensions listed in the caption of Fig.1, and the inter-element spacing is 84 mm. All the MED elements and feeding structure are made of copper sheets with the thickness of 0.3 mm, and each antenna element is fixed to a 190 mm×190 mm substrate by four metal screws.

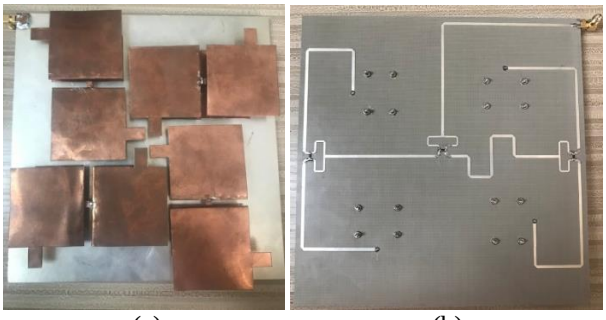

(a) (b)

Fig. 6. The fabricated prototype of the antenna array: (a) top view and (b) two-stage Wilkinson power divider.

The simulated and measured |S11| and AR of the antenna array are presented in Fig. 7. The measured |*S*11| agrees well with the simulated results, and the |*S*11| is less than -10 dB from 1.76 GHz to 2.50 GHz. Agreement of the measured and simulated AR shows good LHCP performance of the array, and the measured 3 dB AR bandwidth is about 32.7% from 1.74 GHz to 2.42 GHz.

Thus, the overlapped |S11| and AR bandwidth is 31.2%, ranging from 1.76 GHz to 2.41 GHz.

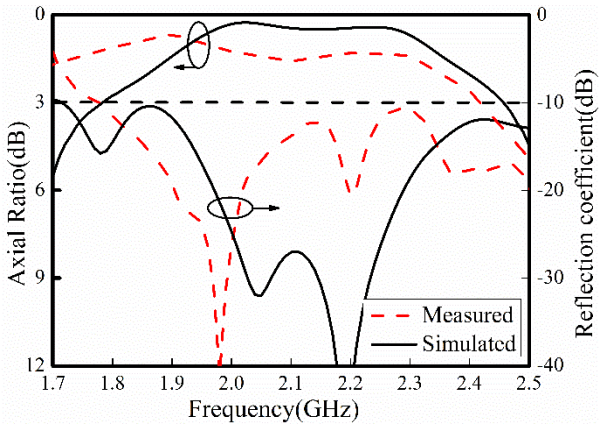

Fig. 7. Simulated and measured reflection coefficient, and axial ratio of the proposed array antenna.

The simulated and measured gain of the antenna array, along with the calculated total efficiency, are illustrated in Fig. 8. The measured peak gain is about 12.9 dBic, and the minimum gain is above 8 dBic within the overlapped bandwidth. The variation of gain is less than 3 dB from 1.85 to 2.32 GHz, showing a bandwidth of 22.5%, which is slightly narrower than the simulated one of 23.1% (1.88-2.37 GHz). It is noted that the maximum difference between the measured results and the simulated ones is about 2 dB, which may be caused by the imprecision of the handmade antenna elements, uncertainties in the measurements, and the losses in the feeding network. The simulated array efficiency is greater than 55% within the entire overlapped bandwidth and more than 72% within the 3 dB gain bandwidth.

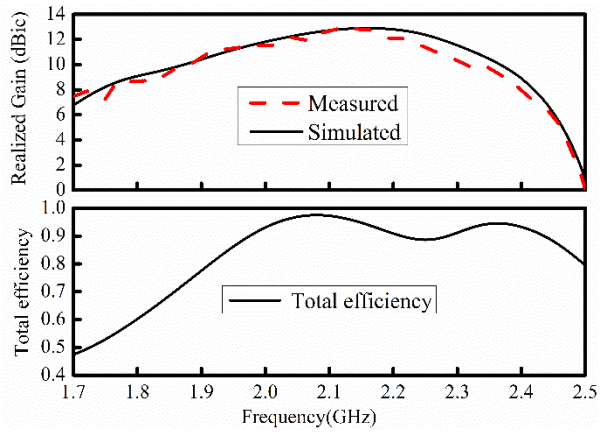

Fig. 8. Simulated and measured realized gain of the array, and simulated total efficiency of the proposed array antenna.

Figure 9 depicts the measured radiation patterns of the array at 1.9, 2.1, and 2.3 GHz, from which good LHCP performance is observed. The simulated results are also plotted for comparison, showing good agreement with the measured ones in the xoz- and yoz-planes. In both planes, the FBR is over 20 dB at each frequency, and the corresponding 3 dB beam-widths in the xoz- and yoz-planes are measured 44.2° and 44.8° at 1.9 GHz, 39.6° and 37.3° at 2.1 GHz, and 37.9° and 36.8° at 2.3 GHz, respectively.

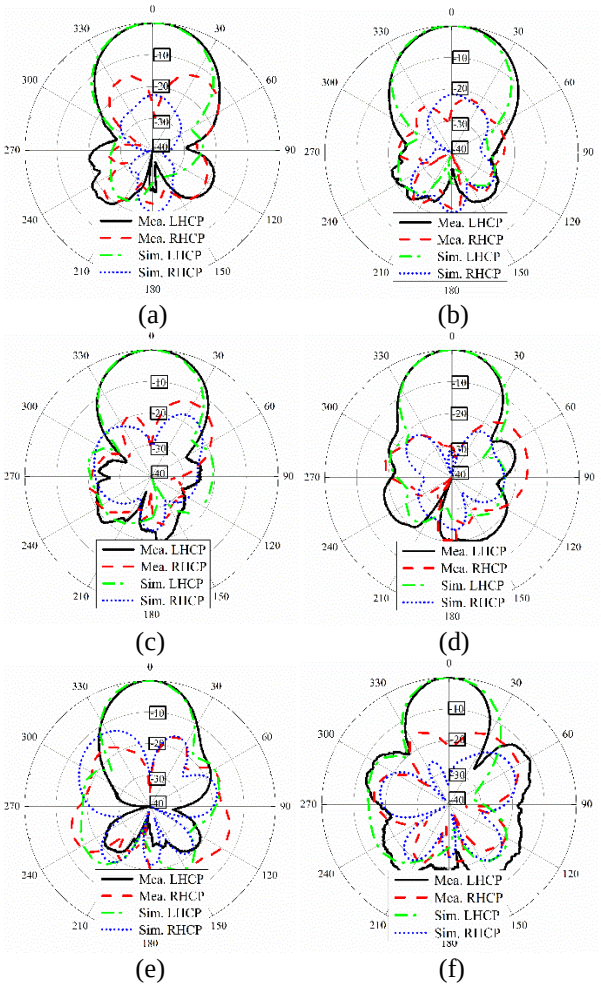

Fig. 9. Simulated and measured radiation patterns of the proposed array antenna at: (a) 1.9GHz at *xz*-plane, (b) 1.9GHz at *yz*-plane, (c) 2.1GHz at *xz*-plane, (d) 2.1GHz at *yz*-plane, (e) 2.3GHz at *xz*-plane, and (f) 2.3GHz at *yz*-plane.

The performance comparison of the proposed CP MED array with other 2×2 arrays that also use the SRF technique is shown in Table 1. Since we did not find other pure metal MED-type 2×2 array designs, it is noted that the comparison arrays listed in Table 1 are all printed on dielectric substrates or substrate- loaded [19-24]. It is seen that the proposed array has wider overlapped

-10 dB |*S*11| and 3 dB AR bandwidth and high gain as compared with these arrays of similar volume sizes. To the best of our knowledge, with similar usable bandwidth, the proposed antenna array has the smallest size among the pure metal MED arrays.

Table 1: Measured results comparisons of the proposed array and other 2×2 arrays with SRF

Array	Overall Size	-10 dB $\lvert S_{11}\rvert$ Bandwidth	3 dB AR Bandwidth	Overlapped Bandwidth	Peak Gain
[19]	$1.45\lambda_c \times 1.45\lambda_c \times 0.028\lambda_c$	15.9%	11.8%	11.8%	12.5 dBic
[20]	$1.32\lambda_c \times 1.32\lambda_c \times 0.065\lambda_c$	36.5%	28.8%	28.8%	13.2 dBic
[21]	$1.82\lambda_c \times 1.82\lambda_c \times 0.040\lambda_c$	>19%	12.7%	12.7%	12.0 dBic
[22]	$1.50\lambda_c \times 1.50\lambda_c \times 0.060\lambda_c$	20.8%	17.6%	17.6%	11.5 dBic
[23]	$1.67\lambda_c \times 1.67\lambda_c \times 0.060\lambda_c$	6.0%	6.8%	6.0%	10.5 dBic
[24]	$2.03\lambda_c \times 2.03\lambda_c \times 0.106\lambda_c$	29.5%	16.2%	16.2%	12.9 dBic
Proposed	$1.33\lambda_c \times 1.33\lambda_c \times 0.070\lambda_c$	34.7%	32.7%	31.2%	12.9 dBic

VI. CONCLUSION

A compact low-profile CP MED antenna array, which is composed of pure metallic structures, is proposed in this paper. The profile of the array is only $0.07\lambda_c$, which is much lower than other pure metal designs of the MED-type. The lateral size of the array is also as small as $1.33\lambda_c \times 1.33\lambda_c$. The measured -10 dB |*S*11| bandwidth is about 35% (1.76-2.5GHz), the 3 dB AR bandwidth is nearly 33% (1.7-2.41 GHz), and the 3 dB gain bandwidth is 22.5% (1.87-2.29GHz) with the peak gain of 12.9 dBic. The proposed array is promising in the applications for portable and individual communication devices.

ACKNOWLEDGMENT

The research and publication of this article was funded by the National Natural Science Foundation of China under Grant [61471040].

REFERENCES

[1] K. M. Luk and H. Wong, "A new wideband unidirectional antenna element," *Int. J. Microw. Opt. Technol.*, vol. 1, no. 1, pp. 35-44, June 2006.

[2] H. Wong, K. M. Mak, and K. M. Luk, "Wideband shorted bowtie patch antenna with electric dipole," *IEEE Trans. Antennas Propag.*, vol. 56, no. 7, pp. 2098-2101, July 2008.

[3] L. Ge and K. M. Luk, "A magneto-electric dipole antenna with low-profile and simple structure," *IEEE Antennas Wireless Propag. Lett.*, vol. 12, pp. 140-142, 2013.

[4] L. Ge and K. M. Luk, "A low-profile magneto-electric dipole antenna," *IEEE Trans. Antennas Propag.*, vol. 60, no. 4, pp. 1684-1689, Apr. 2012.

[5] He K, Gong S, and Gao F, "Low-profile wideband unidirectional patch antenna with improved feed structure," *Electronics Lett.*, vol. 51, no. 4, pp. 317-319, 2015.

[6] K. M. Luk and B. Wu, "The magneto-electric dipole-a wideband antenna for base stations in mobile communications," *Proc. IEEE*, vol. 100, no.7, pp. 2297-2307, 2012.

[7] C. Ding and K. M. Luk, "Low-profile magneto-electric dipole antenna," *IEEE Antennas Wireless Propag. Lett.*, vol. 15, pp.1642-1644, 2016.

[8] M. Li and K.-M. Luk, "A low-profile, low-backlobe and wideband complementary antenna for wireless application," *IEEE Trans. Antennas Propag.*, vol. 63, no. 1, pp. 7-14, Jan. 2015.

[9] M. Li and K.-M. Luk, "A low-profile wideband planar antenna," *IEEE Trans. Antennas Propag.*, vol. 61, no. 9, pp. 4411-4418, Sep. 2013.

[10] C. Y. Shuai and G. M. Wang, "Substrate-integrated low-profile unidirectional antenna," *IET Microw. Antennas Propag.*, vol. 12, no. 2, pp. 185-189, Feb. 2018.

[11] H. W. Lai and H. Wong, "Substrate integrated magneto-electric dipole antenna for 5G wi-fi," *IEEE Trans. Antennas Propag.*, vol. 63, no. 2, pp. 870-874, Feb. 2015.

[12] K. M. Mak and K. M. Luk, "A circularly polarized antenna with wide axial ratio beamwidth," *IEEE Trans. Antennas Propag.*, vol. 57, no. 10, pp. 3309-3312, Oct. 2009.

[13] S. X. Ta and I. Park, "Crossed dipole loaded with magneto-electric dipole for wideband and wide-beam circularly polarized radiation," *IEEE Antennas Wireless Propag. Lett.*, vol. 14, pp. 358-361, 2015.

[14] K. Kang, Y. Shi, and C. H. Liang, "A wideband circularly polarized magneto electric dipole antenna," *IEEE Antennas Wireless Propag. Lett.*, vol. 16, pp. 1647-1650, 2017.

[15] M. Li and K. M. Luk, "A wideband circularly polarized antenna for microwave and millimeter-wave applications," *IEEE Trans. Antennas Propag.*, vol. 62, no. 4, pp. 1872-1879, Apr. 2014.

[16] P.S. Hall, J. S. Dahele, and J. R. James, "Design principles of sequentially fed wide bandwidth circularly polarized microstrip antennas," *in Proc.*

Inst. Elect. Eng., vol. 136, no. 5, pp. 381-389, Oct. 1989.

[17] P. S. Hall, "Application of sequential feeding to wide bandwidth, circularly polarised microstrip patch arrays," *in Proc. Inst. Elect. Eng.*, vol. 136, no. 5, pp. 390-398, Oct. 1989.

[18] C. A. Balanis, *Antenna Theory: Analysis and Design*. 3rd Edition, John Wiley and Sons, New York, 2005.

[19] K. Ding, C. Gao, T. Yu, D. Qu, and B. Zhang, "Gain-improved broadband circularly polarized antenna array with parasitic patches," *IEEE Antennas Wireless Propag. Lett.*, vol. 16, pp. 1468-1471, 2017.

[20] W. Hu, D. Inserra, G. Wen, and Z. Chen, "Wideband low axial ratio and high-gain sequentially rotated antenna array," *IEEE Antennas Wireless Propag. Lett.*, vol. 17, no. 12, pp. 2264-2268, Dec. 2018.

[21] C. Deng, Y. Li, Z. Zhang, and Z. Feng, "A wideband sequential-phase fed circularly polarized patch array," *IEEE Trans. Antennas Propag.*, vol. 62, no. 7, pp. 3890-3893, July 2014.

[22] W. Yang, J. Zhou, Z. Yu, and L. Li, "Bandwidth- and gain-enhanced circularly polarized antenna array using sequential phase feed," *IEEE Antennas Wireless Propag. Lett.*, vol. 13, pp. 1215-1218, 2014.

[23] Y. Li, Z. Zhang, and Z. Feng, "A sequential-phase feed using a circularly polarized shorted loop structure," *IEEE Trans. Antennas Propag.*, vol. 61, no. 3, pp. 1443-1447, Mar. 2013.

[24] M. Akbari, S. Gupta, and A. R. Sebak, "Sequential feeding networks for subarrays of circularly polarized patch antenna," *2016 IEEE Int. Symp. Antennas Propag. (APSURSI)*, Fajardo, pp. 587-588, 2016.